

Electrically Conductive Photoluminescent Porphyrin Phosphonate Metal–Organic Frameworks

Yunus Zorlu, Lukas Wagner, Patrik Tholen, Mehmet Menaf Ayhan, Ceyda Bayraktar, Gabriel Hanna, A. Ozgur Yazaydin, Özgür Yavuzçetin, and Gündoğ Yücesan*

Herein, the design and synthesis of a highly photoluminescent and electrically conductive metal–organic framework [Zn{Cu-*p*-H₆TPPA}]₂[(CH₃)₂NH] (designated as GTUB3), which is constructed using the 5,10,15,20-tetrakis [*p*-phenylphosphonic acid] porphyrin (*p*-H₆TPPA) organic linker, is reported. The bandgap of GTUB3 is measured to be 1.45 and 1.48 eV using diffuse reflectance spectroscopy and photoluminescence (PL) spectroscopy, respectively. The PL decay measurement yields a charge carrier lifetime of 40.6 ns. Impedance and DC measurements yield average electrical conductivities of 0.03 and 4 S m⁻¹, respectively, making GTUB3 a rare example of an electrically conductive 3D metal–organic framework. Thermogravimetric analysis reveals that the organic components of GTUB3 are stable up to 400 °C. Finally, its specific surface area and pore volume are calculated to be 622 m² g⁻¹ and 0.43 cm³ g⁻¹, respectively, using grand canonical Monte Carlo. Owing to its porosity and high electrical conductivity, GTUB3 may be used as a low-cost electrode material in next generation of supercapacitors, while its low bandgap and high photoluminescence make it a promising material for optoelectronic applications.

as paddle wheel patterns.^[6,7] The ligand-binding modes around such molecular IBUs form large angles, ensuring separation between the organic struts and, in turn, resulting in large void spaces.^[11] On the other hand, such separation limits the electrostatic interactions between the organic linkers. Therefore, traditional MOFs lack the required electron hopping and extended conjugation mechanisms between the bridging ligands to support electron mobility.^[12–14] Although high surface area MOFs are ideal platforms to host electrons for supercapacitor applications, due to the lack of such mechanisms, conventional arylcarboxylate MOFs are generally known to be insulators. In addition to electrically conductive MOFs, photoluminescent MOFs have been the subject of active research due to their applications in sensing and light emitting diodes (LEDs).^[15–19] In most cases, the photoluminescence is achieved either by the use of

1. Introduction


Metal–organic frameworks (MOFs) are microporous compounds with a wide range of surface areas, some of which exceed 7000 m² g⁻¹.^[1–3] The majority of MOFs in the literature are synthesized using derivatives of arylcarboxylic acid linkers.^[4–10] Traditional arylcarboxylate MOFs often contain well-defined molecular inorganic building units (IBUs) such

photoluminescent metal ions such as lanthanides, addition of fluorescent dyes to the MOF pores, or ligand exchange.^[17,20] On the other hand, the photoluminescence in MOFs originating purely from the organic moieties is extremely rare and, to the best of our knowledge, there are no electrically conductive MOFs with high photoluminescence in the literature.

Two-dimensional π -stacked MOFs based on ortho-diimine, ortho-dihydroxy, azolate, and thiolate metal-binding groups

Y. Zorlu, M. M. Ayhan, C. Bayraktar
Department of Chemistry
Gebze Technical University
Gebze-Kocaeli 41400, Turkey

L. Wagner
Fraunhofer Institute for Solar Energy Systems ISE
Heidenhofstrasse 2, 79110 Freiburg, Germany

 The ORCID identification number(s) for the author(s) of this article can be found under <https://doi.org/10.1002/adom.202200213>.

© 2022 The Authors. Advanced Optical Materials published by Wiley-VCH GmbH. This is an open access article under the terms of the Creative Commons Attribution-NonCommercial-NoDerivs License, which permits use and distribution in any medium, provided the original work is properly cited, the use is non-commercial and no modifications or adaptations are made.

DOI: 10.1002/adom.202200213

P. Tholen, G. Yücesan
Institute of Food Chemistry and Toxicology
Technische Universität Berlin
Gustav-Meyer-Allee 25, 13355 Berlin, Germany
E-mail: yuecesan@tu-berlin.de

G. Hanna
Department of Chemistry
University of Alberta
116 St. and 85 Ave., Edmonton, Alberta T6G 2R3, Canada

A. O. Yazaydin
Department of Chemical Engineering
University College London
Torrington Place, London WC1E 7JE, UK

Ö. Yavuzçetin
Department of Physics
University of Wisconsin-Whitewater
800 W. Main St., Whitewater WI 53190, USA

have exhibited very high electrical conductivity.^[12,14,21–26] Due to the conservative, strongly chelating metal-binding modes of ortho-diimine and ortho-dihydroxy linkers, these systems are limited to the planar X- and Y-shaped linker geometries. Therefore, efforts to optimize the surface areas and conductivities of these systems have been rather limited. In a similar fashion, it has been very difficult to covalently modify graphene and activated carbon electrode materials to optimize their conductivities and surface areas.^[27] MOFs with metal-binding groups that provide higher structural diversity are required to produce next-generation electrode materials for supercapacitor applications, e.g., use of supercapacitors to reduce the charging time in electrically powered vehicles.^[28,29] In this connection, phosphonates are the most structurally diverse metal-binding groups with three oxygens available for metal-binding in various coordination modes (as shown in Harris notation),^[30–33] In addition, several phosphonate MOFs are known to have exceptionally high thermal and chemical stabilities, which would be beneficial for their use in the presence of water, electrolytes, or even acids.^[34–36] To the best of our knowledge, less than 0.003% of all known MOFs reported in the structural databases are phosphonate MOFs, which are constructed using aromatic phosphonic acid linkers.^[31,37,38] Owing to the aforementioned advantages, phosphonate MOFs may allow for structural variations that generate high electrical conductivity, high photoluminescence and high surface areas for charge holding, and be sufficiently stable for use in industrial applications.

Recently, we reported the first highly stable semiconductive copper-phosphonate MOFs TUB75 and TUB40 with directionally and non-directionally dependent electrical conductivities, respectively, in the 10^{-3} to 10^3 S m^{-1} range.^[39–41] We also reported the first semiconductive permanently microporous hydrogen-bonded phosphonic acid framework (constructed

using the *p*-H₈TPPA linker) with a bandgap of 1.54 eV.^[42] As summarized in a recent review article,^[14] the number of three-dimensional electrically conductive MOFs in the literature is limited. Thus, one of the important goals in MOF chemistry is to synthesize three-dimensional electrically conductive MOFs. Moreover, existing conductive graphene and activated carbon derivatives are known to be carcinogenic and may pose environmental risks.^[43] Thus, another important goal is to synthesize electrically conductive and photoluminescent MOFs that are composed of environmentally safe linkers and metal ions. In this study, we used a porphyrin-cored linker *p*-H₈TPPA (only phosphonic acid protons are included in the formula), which was found to be non-toxic for the osteogenic C2C12 and Caco-2 cell lines,^[44–46] and zinc, which is the second most abundant metal ion found in living systems,^[47] to synthesize a semiconductive zinc-phosphonate MOF named GTUB3. To produce mono-deprotonated phosphonic acid metal-binding groups, we carried out a pH-controlled deprotonation of the Cu-*p*-H₈TPPA linker.^[40] The two mono-deprotonated phosphonate groups in {Cu-*p*-H₆TPPA}^{−2} are involved in the formation of the isolated tetrahedral zinc atoms. Therefore, the zinc atoms can make strong coordinate covalent bonds with non-deprotonated phosphonic acids through the P = O bond and ionic bonds with the mono-deprotonated phosphonic acid tether of {Cu-*p*-H₈TPPA}, giving rise to the simplest tetrahedral ZnO₄ metal-binding modes (where the tetrahedral ZnO₄ IBUs bind to the polyaromatic {Cu-*p*-H₆TPPA}^{−2} linker). The orientation of {Cu-*p*-H₆TPPA}^{−2} in the crystal lattice generates π -stacking between the planar porphyrin units (4.2 Å apart), which may also promote electron hopping (see Figure 1C). Together, these features result in a low bandgap of 1.45 eV and a relatively high average DC electrical conductivity of 4 S m^{-1} (see ref. [14] for a comprehensive list of three-dimensional MOFs and their electrical conductivities).

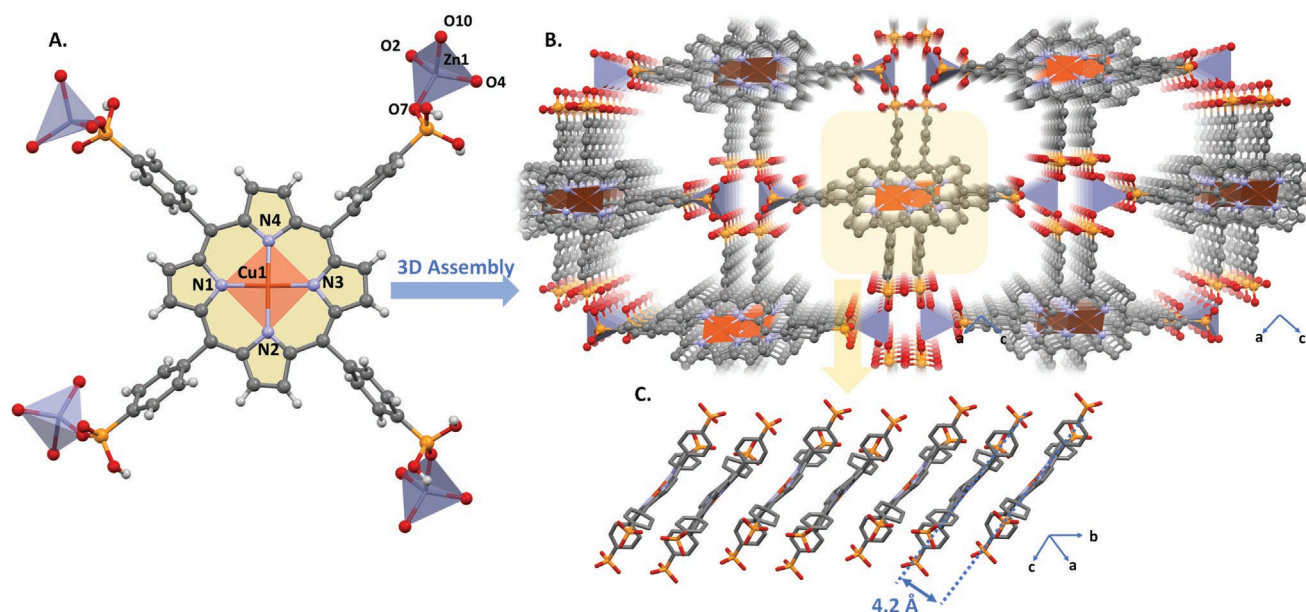


Figure 1. A) Crystal structure of Cu-*p*-H₈TPPA and the zinc coordination modes around the phosphonic acids. B) 3D structure and view of pores in GTUB3. C) Domino-like packing of the porphyrin units in GTUB3, which are separated by 4.2 Å.

2. Results and Discussion

2.1. Synthesis of GTUB3

Due to the rich metal-binding modes of arylphosphonic acids, M-O-M condensations result in unpredictable oligomerizations of metal-phosphonate polyhedra in one, two, and even in three dimensions.^[48,49] Therefore, to achieve predictable synthesis in metal phosphonate chemistry, it is important to restrain the metal-binding modes of phosphonic acids. Many different strategies have been employed to restrain their metal-binding modes such as using phosphonate monoesters and phosphinates.^[31–33,50,51] Recently, we performed the selective mono-deprotonation of arylphosphonic acid using a pH-controlled synthesis to achieve carboxylate-like metal-binding modes in phosphonate MOFs. We adapted the same strategy in this work to reproduce the simplest metal-binding modes observed previously in GTUB4.^[40]

The Cu(*p*-H₈TPPA) linker (see Figure 1A) was synthesized according to our previously reported method (see Figure S3 for the synthetic pipeline).^[40] The single crystals of [Zn{Cu-*p*-H₆TPPA}]·2[(CH₃)₂NH] (GTUB3) were synthesized in scintillation vials after the reaction of 0.03 mmol Zn(NO₃)₂·6H₂O, 0.01 mmol {Cu-*p*-H₈TPPA}, and 1.5 mmol phenylphosphonic acid at 80 °C in the presence of 10 ml:75 ml DMF/H₂O and pH values between 1.7 and 7 (to ensure the limited deprotonation of the phosphonic acids). The yield of the reaction was 90% and the purity of the crystals was confirmed by EDX elemental analysis, ICP-MS, and powder XRD (see Figures S4, S11, and S12-S13, respectively).

2.2. Structure of GTUB3

One of the preferred coordination environments for a zinc atom is tetrahedral. Thus, it is expected that the square planar {Cu-*p*-H₈TPPA} linker will produce a 3D MOF structure when it coordinates to the tetrahedral zinc atom (following the simplest Harris notation).^[30] Figures 1A,B, and C show the structure of GTUB3, which was solved using single-crystal X-ray diffraction (see SI for crystallographic refinement details and Tables S1 and S2 for bond distances). As seen in Figure 1C, the selectively mono-deprotonated phosphonate groups of the {Cu-*p*-H₆TPPA}²⁻ linker coordinate with the tetrahedral zinc atoms to generate a 3D structure. Zinc makes coordinate covalent bonds with the O = P oxygens of the two non-deprotonated phosphonic acid groups, while the mono-deprotonated phosphonate groups of {Cu-*p*-H₆TPPA}²⁻ make ionic bonds with zinc atoms. GTUB3 is unique compared to other 3D phosphonate metal-organic solids with isolated tetrahedral molecular IBUs, as phosphonates are well known to produce complex 1D and 2D IBUs.^[31–33] It has a neutral framework of [Zn(Cu-*p*-H₆TPPA)] and two DMF solvent molecules in the pore sites. The presence of sp²-bound phenylphosphonic acid around the porphyrin core results in extended conjugation throughout the 3D framework. Furthermore, as seen in Figure 1B, the conjugated porphyrin cores of the {Cu-*p*-H₆TPPA}²⁻ linkers in GTUB3 are separated by a distance of ca. 4.2 Å, which leads to electrostatic interactions between each of the porphyrin units and possibly electron

hopping. In addition, the pyrrole ring of the {Cu-*p*-H₆TPPA}²⁻ linker in GTUB3 has a square planar Cu(II) atom, which is known to provide high energy electrons. Finally, the textural properties of GTUB3 were calculated using the Poreblazer v4.0 software.^[37] The N₂-accessible geometric surface area and helium-accessible pore volume of GTUB3 without the solvent molecules are 622 m² g⁻¹ and 0.43 cm³ g⁻¹, respectively. The computed pore size distribution shows that GTUB3's pore widths range from 4 to 7 Å in diameter (see Figure S6).

2.3. Photoluminescence and Bandgap of GTUB3

Photoluminescence (PL) is a process of fundamental importance in solid-state optics. When a photon is absorbed by a semiconductor, an electron can be excited from the ground to an excited electronic state. If the electron and hole recombine radiatively, a photon with energy corresponding to the bandgap is emitted.^[52] In an ideal crystal, all photoexcited charge carriers recombine radiatively, resulting in high PL intensities. In most crystals, however, non-radiative recombination due to high crystal defect densities or indirect bandgaps represents the dominating recombination mechanism (as reflected in reduced PL intensities).^[53,54] In the development of novel semiconductor materials for optoelectronic applications such as light emitting diodes (LEDs) or solar cells, high PL intensities (and hence low non-radiative recombination rates) are essential to achieving high power conversion efficiencies. In this regard, GTUB3 possesses a remarkably high PL intensity. When measured under a PL microscope, the brightest GTUB3 crystals yielded a PL intensity that was more than twice as high as that of a highly efficient perovskite solar cell and six times higher than that of a highly efficient III-V (GaInAsP) solar cell probed under the same setup (see Table 1). However, it should be noted that the PL intensities of full solar cell stacks are usually lower than those of pristine crystal powders. For example, compared to the highly luminescing pristine perovskite (MAPbI₃) powder, the PL of GTUB3 is five times lower. Nevertheless, this is still a highly encouraging result, especially if one considers that GTUB3 has not yet been optimized for optoelectronic applications. Furthermore, we measured the PL quantum yield, defined as the ratio between the radiatively emitted photons and the absorbed photons from the excitation light source. The PL quantum yields of the GTUB3 powder, MAPbI₃ perovskite powder, and perovskite solar cell were found to be 0.091%, 0.698%, and 0.044%, respectively.

Table 1. Photoluminescence (PL) intensities of GTUB3 and other known highly photoluminescent samples, as measured under a PL microscope using a red LED (623 nm peak wavelength) with an intensity of approximately 1 sun (100 mW cm⁻²) to illuminate the sample, and detected through a 760 nm high-pass filter.

Sample	Maximum PL intensity (detector counts, a.u.)
GTUB3 crystal powder	64 744
MAPbI ₃ perovskite crystal powder	321 015
Highly efficient perovskite solar cell	28 217
Highly efficient III-V (GaInAsP) solar cell	11 085

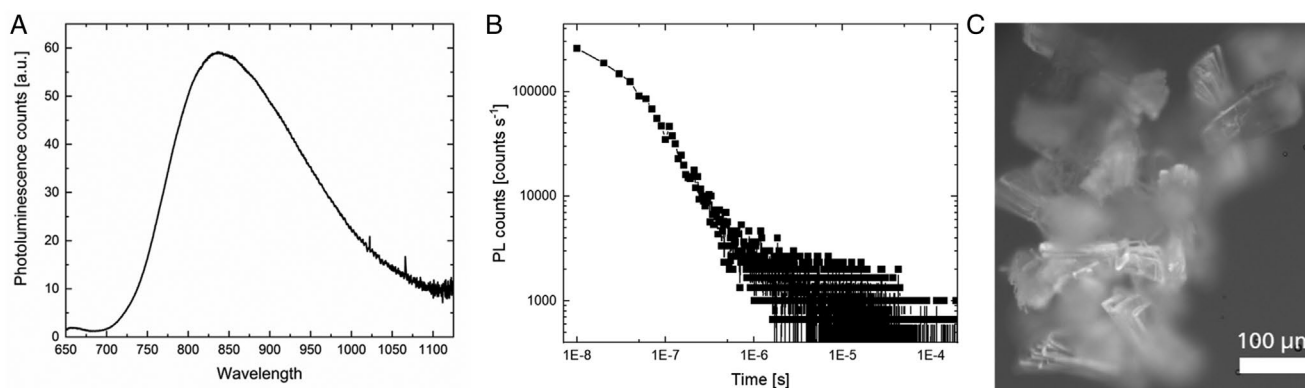


Figure 2. A) Photoluminescence spectrum of GTUB3 crystals upon excitation with a 532 nm laser. B) Measurement of the photoluminescence decay after the excitation laser (515 nm) has been switched off. C) Photoluminescence microscopy image of the GTUB3 crystals displaying the luminescence emission for wavelengths above 760 nm, excited by a red power LED with a peak emission at 623 nm.

Figure 2A displays the PL spectrum of the GTUB3 crystal powder, showing a broad emission with a peak wavelength at 837 nm (1.48 eV). For comparison, the PL spectra of the perovskite powder and perovskite solar cell possess much narrower PL peaks (see Figure S15). Figure 2B displays the results of a PL decay measurement for GTUB3, yielding a PL lifetime of 40.6 ns (assuming a mono-exponential decay) – a promising result for implementation in optoelectronic devices. In comparison, the PL lifetimes of the MAPbI₃ perovskite powder and perovskite solar cell were measured to be 93 ns and 211 ns, respectively (see Figure S14). Such long PL lifetimes are reflective of the long diffusion lengths (on the order of 100 nm to 1 μm) inherent to perovskites.^[55] Long diffusion lengths exceeding the optical absorption depth are an essential criterion for the use of photoabsorber materials in solar cells. A representative PL microscopy image of the GTUB3 crystal powder is shown in Figure 2C.

In addition to the PL work, we generated a Tauc plot of the solid-state diffuse reflectance spectrum (DRS) of the GTUB3 crystal powder to estimate its bandgap (see Figure 3B).^[56] The Tauc plot reveals a bandgap of 1.45 eV, which is in excellent agreement with that extracted from the PL spectrum. The

details of the DRS measurement and Tauc plot fitting may be found in the SI.

2.4. Electrical Conductivity Measurements

To measure the electrical conductivity of GTUB3, we developed a new technique that can quantify the average thickness of the crystals during impedance spectroscopy (the full details of the experimental setup may be found in the SI). This technique is especially useful when the crystal size is less than 1 mm³ and the crystals are randomly oriented and not uniformly covering the electrode surface, which is the case for GTUB3 (see Figure 3A). We used a two-electrode jig system made of mirror-polished and gold-coated copper discs of diameter 12.7 mm and height 6.35 mm. The electrodes were placed between the anvil and spindle of a standard micrometer, insulated by PLA (3D printer filament), and heat-treated for the optimal alignment of the electrodes. We recorded the impedance values (using the Digilent Analog Discovery 2 with impedance analyzer) before and after mounting the samples, for each electrode separation increment/decrement of 0.01mm, between 100Hz-1MHz

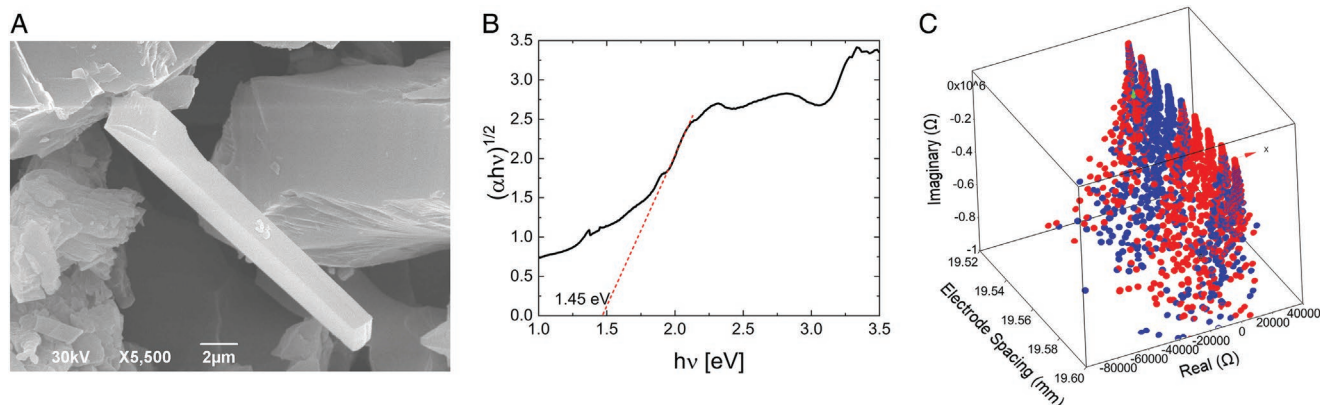


Figure 3. A) SEM pictures of GTUB3 crystals non-uniformly arranged on a surface with random orientations. B) Tauc plot of the diffuse reflectance spectrum of GTUB3, showing an estimate of the bandgap. C) Real and imaginary Nyquist plots of impedance sweeps as a function of electrode spacing (non-offset values). The red- and blue-colored circles correspond to when the electrode gap is closing and opening, respectively.

(as seen in Figure 3C). We estimated the parallel capacitance (which is ca. 8 pF) and offset distance of the electrodes at close proximity and compensated for these factors in the measured values when the sample is mounted. The extrapolation of the Nyquist plots to the real axis yielded a resistance of $\sim 200 \Omega$ (see Figure 3C). Since the conductivity is given by $\sigma = L/RA$ (where L is the length of the sample, R is the resistance, and A is the contact surface area) and $L = 0.08 \text{ mm}$ and $A = 13 \text{ mm}^2$ in our case (estimated from an optical microscope image), we find the conductivity to be $\sigma = 0.03 \text{ S m}^{-1}$. This value represents an estimate of the lower limit of the actual electrical conductivity, as the contact surface area is less than the total surface area of the crystals.

We also performed DC measurements under an optical microscope, by directly pressing on the GTUB3 crystals with a stainless-steel probe attached to a three-axis micromanipulator system connected to a Keithley DMM4050 digital multimeter. After compensating for the probe/wire resistance, we performed ~ 200 random measurements on both single crystals and small crystal bundles in random orientations, yielding resistance values between 100Ω and 300Ω . Due to the small size and fragile nature of the crystals, it was not possible to make measurements exactly along the a -, b -, c -axes of the single crystals; nevertheless, our results show that low resistance values are possible along many (random) directions. Taking this range of resistance values and the surface area of a single crystal to be ca. 0.1 mm^2 (estimated from an optical microscope image), the electrical conductivities were calculated to range between $\sigma = 2 \text{ S m}^{-1}$ and $\sigma = 8 \text{ S m}^{-1}$ with an average of 4 S m^{-1} (based on the average resistance of 200Ω). The relatively high conductivity of GTUB3 may be due to a combination of factors, including electron hopping between the redox active porphyrin units, extended conjugation throughout its 3D structure, the presence of redox-active $p\text{-H}_8\text{TPPA}$ ligands, and high energy square planar Cu(II) d^9 electrons. However, due to the extremely large unit cell of GTUB3 (viz., $13\,189 \text{ \AA}^3$), it would have taken too much computational time/resources to perform electronic structure calculations (at a sufficiently high level of theory for reliable results) to gain deeper insight into these possible factors.

2.5. Thermal Properties

Thermogravimetric analysis (TGA) of GTUB3 shows a two-step weight loss of solvent molecules (DMF) totaling 12.4% (13.8% calculated) until ca. $300 \text{ }^\circ\text{C}$ (see Figure S5). The sharp weight loss beginning at ca. $400 \text{ }^\circ\text{C}$, as seen in the previously reported porphyrin-phosphonate MOFs, indicates the decomposition of the $p\text{-H}_8\text{TPPA}$ linker. The thermal decomposition of GTUB3 continues above $900 \text{ }^\circ\text{C}$, which might be indicative of the formation of heat-stable organophosphide species between 400 and $450 \text{ }^\circ\text{C}$.^[57,58] Therefore, it was not possible to compare the theoretical and calculated weight losses at temperatures above $400 \text{ }^\circ\text{C}$. This unusual decomposition pattern is unique to $p\text{-H}_8\text{TPPA}$ and MOFs constructed using $p\text{-H}_8\text{TPPA}$. For example, similar TGA patterns have also been observed in the thermal decomposition profiles of the starting materials

{Ni- $p\text{-H}_8\text{TPPA}$ } and $p\text{-H}_8\text{TPPA}$, and also GTUB4, a nanotubular $[\text{Ni}\{\text{Cu-}p\text{-H}_4\text{TPPA}\}]^{2-} \cdot 2[(\text{CH}_3)_2\text{NH}_2]^+$ MOF (for a comparison, see Figure S5).^[40,59]

3. Conclusions

Herein, we report on the synthesis and characterization of GTUB3, a semiconductive and photoluminescent 3D zinc-phosphonate MOF. The crystal structure of GTUB3 shows that the polyaromatic $\{\text{Cu-}p\text{-H}_6\text{TPPA}\}^{2-}$ is coordinated to four tetrahedral zinc IBUs and indicates the presence of π -stacking between the porphyrin units. The pyrrole ring of the $\{\text{Cu-}p\text{-H}_6\text{TPPA}\}^{2-}$ core has a square planar Cu(II) atom, which is known to provide high energy electrons. DC measurements reveal a high average electrical conductivity of 4 S m^{-1} , based on measurements along different orientations of the GTUB3 crystals. This makes GTUB3 the first example of an electrically conductive zinc-phosphonate MOF in the literature and a rare example of an electrically conductive 3D MOF. Furthermore, GTUB3 is a highly photoluminescent MOF whose PL exceeds the perovskite solar cells considered in this work. We are currently working on expanding our zinc-phosphonate MOF library using different linker geometries. Due to its porosity, high electrical conductivity, high PL, high-yield synthesis, and low cost, GTUB3 may be used as an electrode material for supercapacitors and in optoelectronic applications.

4. Experimental Section

Data and Materials Availability: All data and details of the synthesis, EDS spectra, electrical conductivity measurements, molecular simulations, X-ray refinement, and bandgap measurement are available in the main text and Supplementary Information. The X-ray crystallographic coordinates for the structure reported in this study can be obtained free of charge from the Cambridge Crystallographic Data Centre (CCDC) [under the deposition number CCDC: 2 052 211 for GTUB3] via www.ccdc.cam.ac.uk/data_request/cif.

Supporting Information

Supporting Information is available from the Wiley Online Library or from the author.

Acknowledgements

G.Y. would like to thank the DFG for funding his work with Grant Number DFG YU 267/2-1. A.O.Y. would like to thank DAAD for supporting his visit to TU-Berlin. A.O.Y. acknowledges the German Academic Exchange Service (DAAD) for funding his visit to TU-Berlin (Grant Number 57 507 438).

Open access funding enabled and organized by Projekt DEAL.

Conflict of Interest

The authors declare no conflict of interest.

Author Contributions

G.Y. created the hypothesis, supervised the project, and wrote the manuscript. Y.Z. synthesized the compound, solved the structure using single-crystal X-ray diffraction, and performed the TGA. L.W. performed the photoluminescence measurements and generated the Tauc plot of the DRS spectrum. P.T. contributed to the crystal structure refinement. A.O.Y. carried out the molecular simulations of the textural properties and wrote the related text. O.Y. took the scanning electron microscope images, designed and constructed the new equipment for measuring the electrical conductivity, measured the conductivity, and wrote the corresponding sections in the manuscript. G.H. provided critical feedback on the results, performed extensive critical revisions of the entire manuscript, and edited the entire manuscript.

Data Availability Statement

The data that support the findings of this study are available in the supplementary material of this article.

Keywords

electrical conductivity, light harvesting layers, metal–organic frameworks, optoelectronics, photovoltaics, semiconductors, supercapacitors

Received: January 29, 2022

Revised: April 4, 2022

Published online:

- [1] O. K. Farha, I. Eryazici, N. C. Jeong, B. G. Hauser, C. E. Wilmer, A. A. Sarjeant, R. Q. Snurr, S. T. Nguyen, A. Ö. Yazaydin, J. T. Hupp, *J. Am. Chem. Soc.* **2012**, *134*, 15016.
- [2] R. Grünker, V. Bon, P. Müller, U. Stoeck, S. Krause, U. Mueller, I. Senkovska, S. Kaskel, *Chem. Commun.* **2014**, *50*, 3450.
- [3] I. M. Hönicke, I. Senkovska, V. Bon, I. A. Baburin, N. Bönisch, S. Raschke, J. D. Evans, S. Kaskel, *Angew. Chem., Int. Ed. Engl.* **2018**, *57*, 13780.
- [4] J. D. Evans, B. Garai, H. Reinsch, W. Li, S. Dissegna, V. Bon, I. Senkovska, R. A. Fischer, S. Kaskel, C. Janiak, N. Stock, D. Volkmer, *Coord. Chem. Rev.* **2019**, *380*, 378.
- [5] H.-C. Zhou, J. R. Long, O. M. Yaghi, *Chem. Rev.* **2012**, *112*, 673.
- [6] O. M. Yaghi, M. O'keeffe, N. W. Ockwig, H. K. Chae, M. Eddaoudi, J. Kim, *Nature* **2003**, *423*, 705.
- [7] M. J. Kalmutzki, N. Hanikel, O. M. Yaghi, *Sci. Adv.* **2018**, *4*, eaat9180.
- [8] S. Yuan, L. Feng, K. Wang, J. Pang, M. Bosch, C. Lollar, Y. Sun, J. Qin, X. Yang, P. Zhang, Q. i Wang, L. Zou, Y. Zhang, L. Zhang, Y. u Fang, J. Li, H.-C. Zhou, *Adv. Mater.* **2018**, *30*, 1704303.
- [9] H. Li, M. Eddaoudi, M. O'keeffe, O. M. Yaghi, *Nature* **1999**, *402*, 276.
- [10] A. Schneemann, V. Bon, I. Schwedler, I. Senkovska, S. Kaskel, R. A. Fischer, *Chem. Soc. Rev.* **2014**, *43*, 6062.
- [11] H. Deng, S. Grunder, K. E. Cordova, C. Valente, H. Furukawa, M. Hmadeh, F. Gándara, A. C. Whalley, Z. Liu, S. Asahina, H. Kazumori, M. O'Keeffe, O. Terasaki, J. F. Stoddart, O. M. Yaghi, *Science* **2012**, *336*, 1018.
- [12] L. Sun, M. G. Campbell, M. Dincă, *Angew. Chem., Int. Ed.* **2016**, *55*, 3566.
- [13] G. Skorupskii, B. A. Trumpf, T. W. Kasel, C. M. Brown, C. H. Hendon, M. Dincă, *Nat. Chem.* **2020**, *12*, 131.
- [14] L. S. Xie, G. Skorupskii, M. Dincă, *Chem. Rev.* **2020**, *120*, 8536.
- [15] Y. Tang, W. Cao, L. Yao, Y. Cui, Y. Yu, G. Qian, J. *Mater. Chem. C* **2020**, *8*, 12308.
- [16] M. Gutiérrez, C. Martín, M. Van Der Auweraer, J. Hofkens, J.-C. Tan, *Adv. Opt. Mater.* **2020**, *8*, 2000670.
- [17] J. Dong, D. Zhao, Y. Lu, W.-Y. Sun, *J. Mater. Chem. A* **2019**, *7*, 22744.
- [18] Z. Hu, B. J. Deibert, J. Li, *Chem. Soc. Rev.* **2014**, *43*, 5815.
- [19] M. D. Allendorf, C. A. Bauer, R. K. Bhakta, R. J. T. Houk, *Chem. Soc. Rev.* **2009**, *38*, 1330.
- [20] M. Pamei, A. Puzari, *Nano-Struct. Nano-Objects* **2019**, *19*, 100364.
- [21] L. S. Xie, E. V. Alexandrov, G. Skorupskii, D. M. Proserpio, M. Dincă, *Chem. Sci.* **2019**, *10*, 8558.
- [22] D. Sheberla, J. C. Bachman, J. S. Elias, C.-J. Sun, Y. Shao-Horn, M. Dincă, *Nat. Mater.* **2017**, *16*, 220.
- [23] J.-H. Dou, M. Q. Arguilla, Y. Luo, J. Li, W. Zhang, L. Sun, J. L. Mancuso, L. Yang, T. Chen, L. R. Parent, G. Skorupskii, N. J. Libretto, C. Sun, M. C. Yang, P. V. Dip, E. J. Brignole, J. T. Miller, J. Kong, C. H. Hendon, J. Sun, M. Dincă, *Nat. Mater.* **2021**, *20*, 222.
- [24] R. Dong, Z. Zhang, D. C. Tranca, S. Zhou, M. Wang, P. Adler, Z. Liao, F. Liu, Y. Sun, W. Shi, Z. Zhang, E. Zschech, S. C. B. Mannsfeld, C. Felser, X. Feng, *Nat. Commun.* **2018**, *9*, 2637.
- [25] K. W. Nam, S. S. Park, R. Dos Reis, V. P. Dravid, H. Kim, C. A. Mirkin, J. F. Stoddart, *Nat. Commun.* **2019**, *10*, 4948.
- [26] X. Huang, H. Yao, Y. Cui, W. Hao, J. Zhu, W. Xu, D. Zhu, *ACS Appl. Mater. Interfaces* **2017**, *9*, 40752.
- [27] A. J. Clancy, H. Au, N. Rubio, G. O. Coulter, M. S. P. Shaffer, *Dalton Trans.* **2020**, *49*, 10308.
- [28] W.-H. Li, K. Ding, H.-R. Tian, M.-S. Yao, B. Nath, W.-H. Deng, Y. Wang, G. Xu, *Adv. Funct. Mater.* **2017**, *27*, 1702067.
- [29] J. Liu, X. Song, T. Zhang, S. Liu, H. Wen, L. Chen, *Angew. Chem., Int. Ed. Engl.* **2021**, *60*, 5612.
- [30] R. A. Coxall, S. G. Harris, D. K. Henderson, S. Parsons, P. A. Tasker, R. E. P. Winpenny, *J. Chem. Soc., Dalton Trans.* **2000**, *14*, 2349.
- [31] G. Yücesan, Y. Zorlu, M. Stricker, J. Beckmann, *Coord. Chem. Rev.* **2018**, *369*, 105.
- [32] S. J. I. Shearan, N. Stock, F. Emmerling, J. Demel, P. A. Wright, K. D. Demadis, M. Vassaki, F. Costantino, R. Viviani, S. Sallard, I. R. Salcedo, A. C. M. Taddei, *Crystals* **2019**, *9*, 5.
- [33] K. J. Gagnon, H. P. Perry, A. Clearfield, *Chem. Rev.* **2012**, *112*, 1034.
- [34] C.-Y. Gao, J. Ai, H.-R. Tian, D. Wu, Z.-M. Sun, *Chem. Commun.* **2017**, *53*, 1293.
- [35] T. Zheng, Z. Yang, D. Gui, Z. Liu, X. Wang, X. Dai, S. Liu, L. Zhang, Y. Gao, L. Chen, D. Sheng, Y. Wang, J. Diwu, J. Wang, R. Zhou, Z. Chai, T. E. Albrecht-Schmitt, S. Wang, *Nat. Commun.* **2017**, *8*, 15369.
- [36] Y. Zorlu, D. Erbahar, A. Çetinkaya, A. Bulut, T. S. Erkal, A. O. Yazaydin, J. Beckmann, G. Yücesan, *Chem. Commun.* **2019**, *55*, 3053.
- [37] L. Sarkisov, R. Bueno-Perez, M. Sutharson, D. Fairen-Jimenez, *Chem. Mater.* **2020**, *32*, 9849.
- [38] C. E. Wilmer, M. Leaf, C. Y. Lee, O. K. Farha, B. G. Hauser, J. T. Hupp, R. Q. Snurr, *Nat. Chem.* **2012**, *4*, 83.
- [39] K. Siemensmeyer, C. A. Peeples, P. Tholen, F.-J. Schmitt, B. Çoşut, G. Hanna, G. Yücesan, *Adv. Mater.* **2020**, *32*, 2000474.
- [40] M. M. Ayhan, C. Bayraktar, K. B. Yu, G. Hanna, A. O. Yazaydin, Y. Zorlu, G. Yücesan, *Chemistry* **2020**, *26*, 14813.
- [41] C. A. Peeples, D. Kober, F.-J. Schmitt, P. Tholen, K. Siemensmeyer, Q. Halldorson, B. Çoşut, A. Gurlo, A. O. Yazaydin, G. Hanna, G. Yücesan, *Adv. Funct. Mater.* **2021**, *31*, 2007294.
- [42] P. Tholen, C. A. Peeples, R. Schaper, C. Bayraktar, T. S. Erkal, M. M. Ayhan, B. Çoşut, J. Beckmann, A. O. Yazaydin, M. Wark, G. Hanna, Y. Zorlu, G. Yücesan, *Nat. Commun.* **2020**, *11*, 3180.
- [43] R. Arvidsson, M. Boholm, M. Johansson, M. L. De Montoya, *Nanoethics* **2018**, *12*, 199.
- [44] M. Maares, M. M. Ayhan, K. B. Yu, A. O. Yazaydin, K. Harmandar, H. Haase, J. Beckmann, Y. Zorlu, G. Yücesan, *Chem. - Eur. J.* **2019**, *25*, 11214.

- [45] C. Keil, J. Klein, F.-J. Schmitt, Y. Zorlu, H. Haase, G. Yücesan, *Chem-BioChem* **2021**, 22, 1925.
- [46] Y. Zorlu, C. Brown, C. Keil, M. M. Ayhan, H. Haase, R. B. Thompson, I. Lengyel, G. Yücesan, *Chemistry* **2020**, 26, 11129.
- [47] W. Maret, *Metallomics* **2014**, 6, 1174.
- [48] A. Bulut, M. Wörle, Y. Zorlu, E. Kirpi, H. Kurt, J. Zubieta, S. Grabowsky, J. Beckmann, G. Yücesan, *Acta Crystallogr., Sect. B: Struct. Sci., Cryst. Eng. Mater.* **2017**, 73, 296.
- [49] G. Cao, H. G. Hong, T. E. Mallouk, *Acc. Chem. Res.* **1992**, 25, 420.
- [50] J. Hynek, P. Brázda, J. Rohlíček, M. G. S. Londesborough, J. Demel, *Angew. Chem., Int. Ed.* **2018**, 57, 5016.
- [51] D. Bůžek, S. Ondrušová, J. Hynek, P. Kovář, K. Lang, J. Rohlíček, J. Demel, *Inorg. Chem.* **2020**, 59, 5538.
- [52] A. Einstein, *Physik. Z.* **1917**, 18, 121.
- [53] P. Caprioglio, M. Stolterfoht, C. M. Wolff, T. Unold, B. Rech, S. Albrecht, D. Neher, *Adv. Energy Mater.* **2019**, 9, 1901631.
- [54] P. K. Nayak, S. Mahesh, H. J. Snaith, D. Cahen, *Nat. Rev. Mater.* **2019**, 4, 269.
- [55] S. D. Stranks, G. E. Eperon, G. Grancini, C. Menelaou, M. J. P. Alcocer, T. Leijtens, L. M. Herz, A. Petrozza, H. J. Snaith, *Science* **2013**, 342, 341.
- [56] J. Tauc, R. Grigorovici, A. Vancu, *Phys. Status Solidi* **1966**, 15, 627.
- [57] T. Yi, et al., *Inorg. Chem.* **2013**, 52, 3787.
- [58] R. Zhang, et al., *ACS Appl. Mater. Interfaces* **2017**, 9, 14013.
- [59] Y. Y. Enakieva, A. A. Sinelshchikova, M. S. Grigoriev, V. V. Chernyshev, K. A. Kovalenko, I. A. Stenina, A. B. Yaroslavtsev, Y. G. Gorbunova, A. Y. Tsivadze, *Chem. – Eur. J.* **2019**, 25, 10552.